DM and the MW 511 keV Signal: Using a Radially Dependent XDM Model to Constrain the WIMP Mass with INTEGRAL/SPI

Michael Jafs[1, *]

[1]*Department of Physics, Engineering Physics and Astronomy, Queen's University, Kingston, ON K7L 3N6, Canada*
(Dated: April 11, 2022)

The problem of an excess amount of 511 keV emission, with a peaked intensity in the Galactic bulge is examined in-depth. We provide a detailed account of the 511 keV spectrum, it's distribution in the Milky Way, and discuss various observations that have contributed to mapping this gamma-ray signal. We give a detailed description of the candidate sources which have been most studied and outline how a DM origin, specifically one involving the more recent excited dark matter (XDM) model, may be the most probable explanation for the observed emission. We outline the results and methodology of earlier work, which has gone into explaining the emission profile with a dark matter origin. Using an NFW profile and halo parameters consistent with N-body simulations, we incorporate a radial dependence into the annihilation rate coefficient and compare our model profile directly to the most recent data from INTEGRAL/SPI. Using a least squares regression, we are able to constrain both the WIMP mass and the normalization constant in our annihilation rate coefficient. Our best fit results produce a WIMP mass of $\sim$ 2861 GeV, which could align with the current expected WIMP range of $\sim$GeV-TeV, caused by the lack of a signal, in current direct detection experiments.

I. INTRODUCTION

For the last few decades, an emission line signal at 511 keV has puzzled many researchers. The signal, with a large intensity at the Galactic center, has a peak in it's spectrum at exactly 511 keV, with a continuum at large and smaller energies. Since the earliest gamma-ray observations of the Galactic center have been able to provide a clear enough picture of the signal's morphology and intensity, no theories of what is causing the signal have been successful in describe all of it's characteristics.

The 511 emission line itself, is thought to be the result of positronium annihilation, since the annihilation of the parapositronium state results in two photons, both with energy equal to 511 keV, however the continuum above and below this line is less well understood. Attempts at describing the signal include the discussion of radioactive decay, since the β^+ decay of radioactive elements produced by various astrophysical sources produces positrons. The black hole at the center of the milky way has even been proposed as a candidate for producing various characteristics of the observed 511 keV signal. Perhaps the most intriguing of theories being used to describe the signal are those involving dark matter. The dark matter halo profile has been shown to have a large density concentration in the Galactic center, where the flux of 511 keV emission is the largest. This is just one example motivating dark matter as a theory to described the strange excess of emission.

This paper explores the still miss-understood problem regarding an excess of 511 keV emission in the Galactic center and proposes a solution in the form of excited dark matter (XDM). The structure of this report is as follows. In Section II A, we provide a discussion of the 511 keV signal, and how it relates to the Milky Way. We then outline the various candidate sources proposed as a solution thus far

in, Sec. II B. We examine the methodology and results of a few efforts which have tried to explain the signal using DM as an origin source in Sec. II C. In Sec. III, we outline our contribution to some of the earlier models mentioned in the previous section and give a detailed account of our theoretical model. We provide the results of our own model in Sec. IV and discuss many of the implications of our results in Sec. V. Finally, Sec. VI provides concluding remarks.

II. BACKGROUND AND EARLIER WORK

A. The Milky Way 511 KeV Signal

Basic conservation laws tell us that the annihilation of $e^- e^+$ (electron positron) pairs should produce a signal at 511 keV. In other words, the interaction $e^- e^+ \rightarrow \gamma\gamma$ does not violate any conservation laws. Each photon must additionally carry away a frequency of 511 keV in order to conserve energy. What we have just described is the case of direct annihilation of $e^- e^+$ pairs at rest [1]. $e^- e^+$ pairs can also exist in a bound system called positronium and will eventually self annihilate resulting in a composite spectrum with a lower energy continuum and a 511 keV line [1]. The bound positronium state consists of two separate states which are defined by whether the spins are aligned (para-positronium or p-Ps) or anti-aligned (ortho-positronium or o-Ps). Spin degeneracy, causes o-Ps to be formed 3/4 of the time, while p-Ps is formed 1/4 of the time. P-Ps releases two photons of 511 keV in opposite directions, while the o-Ps state requires a final state with more than two photons, resulting in a continuum of energies which add ip to 511 keV [1].

Fig 1 shows the spectrum of 511 keV emission confined to the bulge of the MW (Milky Way). The o-ps continuum is visible for energies < 511 keV. There is also a γ-ray continuum for energies larger than 511 keV which is visible in Fig. 1. This is sometimes referred as the MeV con-

tinuum and is caused by relativistic positrons annihilating "in-flight", the center of mass energy allowing the photons to carry away energies >511 keV. The 511 line spectrum differs slightly in the disk when compared to the bulge. In the 511 keV disk spectrum, the o-Ps continuum is less obvious and the diffuse γ-ray spectrum more pronounced. Ref [2] interprets this as a disk annihilation signature that is subdominant when looking towards the GC due to other components with large surface brightnesses.

The shape and amplitude of the MeV continuum depends on the injection spectrum and annihilation rate [1]. Similarly, the positronium fraction (f_{Ps}) can be derived from the intensity of both the 511 keV line, and the o-Ps continuum. Since positronium formation is only efficient at energies less than roughly 100 eV and is assisted by charge exchange interaction in a partially neutral medium, the nature of the surrounding medium can be understood by determining the positronium fraction [2].
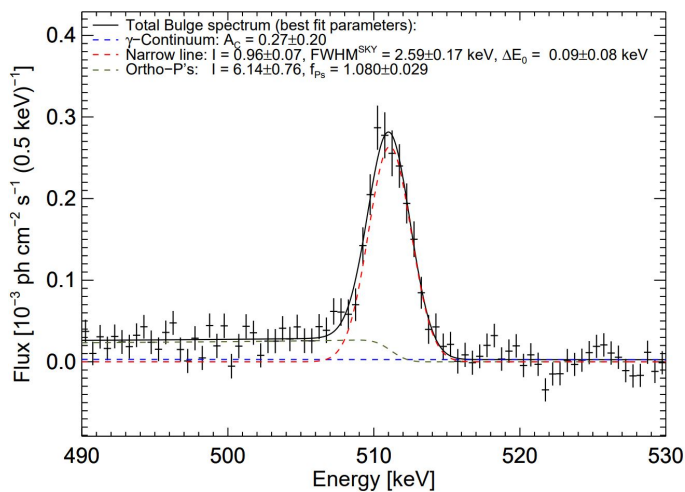

Figure 1. Spectrum of 511 keV emission in the Galactic bulge. The best fit to the experimental data is given as the black line and is made up of the annihilation line (red dashed), the o-Ps line (olive dashed), and the diffuse MeV continuum (dashed blue). From [2].

The earliest measurements of 511 keV radiation in the Milky Way were obtained through various balloon flights in the 1970's. By directing their field of view toward the Galactic center, most of the experiments were able to confirm there was a signal lying close to the proposed 511 keV. The source of the e^+ emission was unclear, however research teams began to consider the fact that the resulting emission may be caused by sources such as β^+ decay from elements produced in supernovae. In each case, there was found to be a flux of radiation of $\sim 10^{-3}$ ph cm^{-2} s^{-1}. In 2002, an opportunity for better measurements of Galactic e^+ annihilation came from the launch of the International Gamma-Ray Astrophysics Observatory (INTEGRAL) with imaging from the on board spectrometer SPI. Prior to INTEGRAL, measurements were made with instruments such as OSSE on board CGRO (Compton Gamma Ray Observatory) with collimators with a field of view (FoV) of 3.8 by 11 degrees [2]. SPI is capable of imaging with up to 2 degrees of precision with its coded mask technique. The launch of INTEGRAL also saw the first

all-sky images of the Galactic 511 keV emission [3, 4]. The INTEGRAL survey's exposure also more effectively covers the entire inner galaxy [2]. An example of the exposure map from one of the latest SPI data sets (and the data we compare our model to in Section IV B) can be seen in Fig. 2. This figure represents $\sim$11 years of γ-ray observations in SPI's 20 keV to 8 MeV range and demonstrates the spacial extent of observations in INTEGRAL's ongoing mission.

Similar experiments such as COMPTEL on board CGRO, have carried out all-sky surveys, however, COMPTEL was focused on observations of γ-ray emission from the decay of ^{26}Al. ^{26}Al releases a positron when it decays, while the de-excitation of its daughter nucleus produces a characteristic γ-ray line at 1808.63 keV [1]. When considering the constraints placed on positron formation and annihilation in the MW from the INTEGRAL survey and other observations, results of analysis from Ref [1] show that the total positron annihilation rate observed in γ-rays is greater than $\sim 10^{42}$ s^{-1} and is mostly confined to the bulge. Ref [1] also finds there to be a bulge/disk ratio of $\sim$1.4. Additionally, the ratio of the 511 keV line to the continuum emission places a constraint on the positronium fraction of 97$\pm$2%. It is therefore measurements of these parameters which serve to constrain the physical conditions in the location of 511 keV emission.
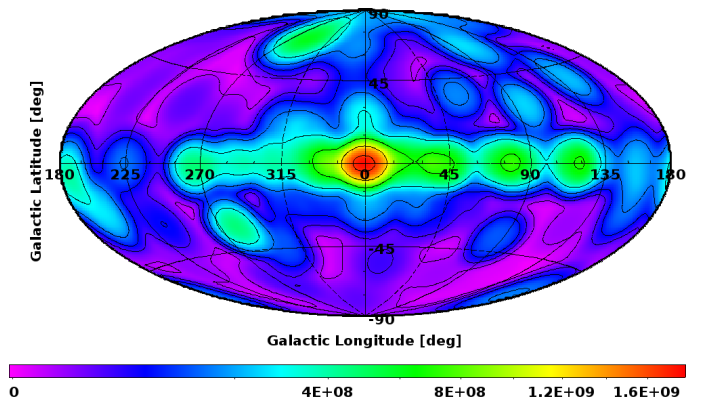

Figure 2. Exposure map from SPI data collection from the data set in [2]. The contours correspond to exposures of 22 Ms, 16 Ms, 9 Ms, 4 Ms, 2 Ms, 1 Ms, 0.5 Ms, and 0.1 Ms. From [2].

B. Candidate Sources

The various candidate sources that have been explored in depth are reviewed in [1]. The first of these is radioactive decay from stellar nucleosynthesis caused by sources throughout the MW. β^+ decay of unstable isotopes results in positrons that are of order MeV in energy[1], a necessary ingredient if we are to observe the diffuse γ-ray emission in the 511 keV spectrum. ^{26}Al can be produced in both the H-burning phase and during the supernova phase of a high-mass stars lifetime [5]. Additionally, ^{44}Ti is produced deep in a supernova's layers [6]. In even more energetic events such as hypernovae and gamma ray bursts, ejected ^{56}Ni masses can be on the order of 0.5 M$_\odot$ [7]. In the case of Hypernovae/GRB, Ref [1] explains that candidate

Source	Process	$E(e^+)^a$ (MeV)	e^+ rate^b $\dot{N}_{e+}$ $(10^{43}$ s$^{-1})$	Bulge/Disk^c B/D	Comments
Massive stars: ^{26}Al	β^+-decay	~ 1	0.4	<0.2	$\dot{N}, B/D$: Observationally inferred
Supernovae: ^{24}Ti	β^+-decay	~ 1	0.3	<0.2	$\dot{N}$: Robust estimate
SNIa: ^{56}Ni	β^+-decay	~ 1	2	<0.5	Assuming $f_{e+,esc}$=0.04
Novae	β^+-decay	~ 1	0.02	<0.5	Insuffient e^+ production
Hypernovae/GRB: ^{56}Ni	β^+-decay	~ 1	?	<0.2	Improbable in inner MW
Cosmic rays	p-p	~ 30	0.1	<0.2	Too high e^+ energy
LMXRBs	$\gamma - \gamma$	~ 1	2	<0.5	Assuming $L_{e+} \sim 0.01 \, L_{obs,X}$
Microquasars (μQs)	$\gamma - \gamma$	~ 1	1	<0.5	e^+ load of jets uncertain
Pulsars	$\gamma - \gamma \,/\, \gamma - \gamma_B$	>30	0.5	<0.2	Too high e^+ energy
ms pulsars	$\gamma - \gamma \,/\, \gamma - \gamma_B$	>30	0.15	<0.5	Too high e^+ energy
Magnetars	$\gamma - \gamma \,/\, \gamma - \gamma_B$	>30	0.16	<0.2	Too high e^+ energy
Central black hole	p-p	High	?		Too high e^+ energy, unless B >0.4 mG
	$\gamma - \gamma$	1	?		Requires e^+ diffusion to ~ 1 kpc
Dark matter	Annihilation	1 (?)	?		Requires light scalar particle, cuspy DM profile
	Deexcitation	1	?		Only cuspy DM profiles allowed
	Decay	1	?		Ruled out for all DM profiles
Observational constraints		<7	2	>1.4	

Figure 3. Possible positron emitting candidates and their properties. From [1].

sources produce positrons through radioactive decay of the unstable ^{56}Ni decay, or through pair creation as ionized photons interact with the GRB photons. Type 1-a supernoave (SNIa) and novae can also produce radio active elements in the form of ^{56}Ni and even ^{13}N, ^{18}F (produced in the CNO cycle) and ^{22}Na in the NeNa cycle [1]. Although ^{13}N and ^{18}F are known e^+ producers, they are not likely to travel out of their hot nova ejecta, however e^+ from ^{28}Na decay has been shown [1] to result in a Galactic e^+ production rate of $\sim 1.5 \times 10^{41}$ s^{-1}. Ref [8] looked at e^+ emission from decay of ^{26}Al, ^{56}Ni, and ^{44}Ti and found that nucleosynthesis positrons cannot account for the morphology and intensity seen in the bulge, but can account for the properties of the 511 keV spectrum seen in the disk. Although each of these radioactive sources contribute at a non-negligible level to the Galactic e^+ production rate [1], the uncertainties in these measurements are large and they fail to produce the necessary B/D (bulge to disk) ratio.

The second set of candidate sources Ref [1] summarizes are those involving highly energetic processes and compact objects. Relativistic protons can produce e^+ through secondary positrons [1], the majority of which can be traced back to a cosmic ray origin. Pair production ($\gamma\gamma \rightarrow e^- e^+$) is also possible when the product of the photon energies is large. In very large magnetic field regions produced in the vicinity of pulsars and megnetars, pair production of a $e^- e^+$ pair is possible from a single photon [9]. According to Ref [1], pulsars and magnetars have a distribution akin to star forming regions and do not have a major bulge contribution. Millisecond Pulsars, should have a significant bulge component however, with a B/D ratio <0.5. The diffuse continuum observed in the 511 KeV emission spectrum constrains the flux of emission in the higher energy regime, meaning that these very high energy compact sources (with injection energies ~ 30 MeV [1]) produce e^+ with energies far too high to result in the observed diffuse emission.

Another possibility is X-ray binaries (XRBs) or micro-

quasars. The e^+ production mechanisms here, are additionally those of pair production due to the jets associated with these compact objects. Microquasar jets have been shown to have sufficient luminosity and can in fact yield the necessary e^+ production rate [10]. Additionally, low mass x-ray binaries (LMXRBs), were shown to have a distribution peaked toward the bulge with a total luminosity well capable of resulting in the necessary e^+ production rate. [11]. However, these results should be taken more as optimistic results, since assumptions of e^+ production rates are still very highly uncertain [1]. Furthermore, the morphology of the observed emission may favour LMXRBs and microquasars, but the highly energetic pair creation positrons contradict the diffuse γ-ray part of the 511 keV spectrum.

Ref [1] also mentions that Sgr A*, the super massive black hole at the GC, has been suggested as a possible e^+ emitting source that has potential to produce the signal observed. The positrons could be produced as either secondary positrons (from pp collisions when protons are accelerated by the SMBH) or by pair production. In each case, various models have been constructed in an effort to have the proposed e^+ production rate from Sgr A* accurately describe the observed 511 keV signal. In all cases, it seems that the observed morphology and required injection energy are again difficult to model using the SMBH as a e^+ producing source alone.

The final candidate summarized in some depth by [1] is a source involving dark matter (DM) or another, more exotic type of non-standard source. The notion of "weakly interacting massive particles" or WIMPs has been used to describe the collision-less matter that seems to be a necessary ingredient if we are to describe many kinematic properties of the universe. Specifically, DM's absence of electric charge, deems it weakly interacting, but with a lower limit set on its mass by what is known as a "free-streaming effect" [1]. Therefore, DM likely isn't massless. In fact, DM in the GeV to TeV range agrees with the absence of a pos-

itive signal in current direct detection experiments. The DM mass can be constrained by assuming a decaying or annihilating scenario resulting in e^+ formation under the assumption that the positrons will annihilate in-flight and contribute to the diffuse γ-ray continuum. Moreover, an upper mass limit can be placed on DM by the assumption that the disk emission is well understood and that the excess emission may be due to a DM source.

These constraints have led to investigations involving light DM annihilating [12, 13] and decaying scenarios. Though the light WIMP scenario was shown to be highly ruled out by Ref [14]. They have also led to the proposal of an excited DM (XDM) scenario [12, 15] in which DM particles in the heavy mass (GeV-TeV) range, capable of an excited state, de-excite after an inelastic collision, resulting in a $e^- e^+$ pair. According to Ref [1], the light decaying DM scenario was introduced to try and explain the low energy positron distribution in the bulge as seen by SPI observations. Since this proposal, the low mass (<100MeV) DM particle candidate has been shown to be highly disfavoured when constrained by observations. In fact, we show the results of several investigations [12–14] which have led to this conclusion (Section II C). The necessary injection energy of e^+ seems to play a large part it limiting the capability of purely annihilating and decay DM. Since SPI observations provide a good picture of the diffuse γ-ray spectrum, there is an upper mass limit on DM candidates in this scenario.

The morphology of the e^+ distribution however, allows for a promising result for DM candidates of all types, since recent models of the DM MW density profile (Eg. [16]), representative of the DM halo, show a high density in the bulge when compared to the disk. Data sets from INTE-GRAL/SPI [2] can be used to constrain various DM models for different proposed density profiles. For example, as has been done by Refs [12, 13]. Ref [1] mentions that in the decaying scenario, the flux profile is too flat compared to SPI data. Whereas annihilating and XDM models produce a flux that is much more peaked in the GC, which better aligns with SPI data. Unfortunately, even though the DM halo and the flux of emission from the 511 keV line seem to share the GC as a high density region, there are still many uncertainties surrounding these conclusions. For example, contamination from other astrophysical sources may still play a large part in the density of positrons in the GC. Nevertheless, DM scenarios remain an interesting and prospective source of the 511 line flux due to the simulations involving the DM halo profile. Specifically, the XDM model may provide the most promising candidate due to it's ability to describe more of the observed spectra (not being limited to low mass WIMPs).

What we have neglected to discuss in any detail thus far is the notion of positron transport in the MW. All of the above discussion heavily relies on the idea that positrons likely do not annihilate far from their source distribution. Some work has gone into studying propagation of positrons (Eg. [17]) but it seems that it is not likely that Galactic positrons propagate at distance scales far enough for the astrophysical sources discussed in this section to result in the observed emission. Ref [2] mentions that if there does happen to be significant positron transport (scales ~kpc) that positrons will still annihilate when they reach

denser, warm cloud phases. Indicating that the e^+ distribution is therefore more representative of the warm cloud phases, rather than the source distribution. Fig. 3 outlines the sources discussed in this section and comments on the main problems/inconsistencies/constraints present for each candidate source. Clearly, the the observed flux of 511 keV emission presents a puzzling scenario and still requires much work if we are to conclusively determine the source of this emission spectra. The rest of this report will focus on work which has been done involving DM to explain the 511 keV flux, with an emphasis on the most promising solution. That of excited dark matter.

C. Positron Production Models via Dark Matter

We have already discussed the various DM candidates that have been used to try and explain the 511 keV signal, however, in this section we outline the methodology and results of a few investigations involving DM explanations to the signal. As mentioned in Section II B, three main proposals involving DM have been used to try and explain the flux of e^+ annihilation. These are light WIMPs (<100MeV) that either annihilation or decay, or heavy WIMPs (GeV-TeV) that take part in the XDM model.

Some of the earliest work was done by Ref [13] when early data sets from INTEGRAL/SPI allowed for comparison between theoretical models and experimental observations. Their work focused on the annihilating and decaying DM scenario, originally thought to be able to produce characteristics of the observed signal. They quote that there is agreement that a universal function with a small number of free parameters should be capable of describing the DM halo profile. They refer to a generalized profile, which in their paper they write as:

$$\rho(r) = \frac{\rho_0}{(r/r_0)^\gamma [1 + (r/r_0)^\alpha]^{(\beta-\gamma)/\alpha}}, \qquad (1)$$

where ρ_0, r_0, and γ are the characteristic density, characteristic radius, and slope parameter respectively. β and α are fit parameters which control the shape of the profile for different values of the Galactic radius r. In the case of the famous Navarro-Frenk-White (NFW) profile [16], $\alpha = 1$, $\beta = 3$, $\gamma = 1$, $r_0 = 16.7$ kpc, and $\rho_0 = 0.347$ GeV cm^{-3}, according to Ref [13]. The work done by Ref [13] also takes into account, the fact that the e^+ production rate from DM depends on the velocity of the DM particles. They motivate the DM cross-section used across many of the DM e^+ producing models, $\langle \sigma v \rangle$. The number density of DM particles, n_{dm}, times their rate of decay or annihilation produces the number of expected e^+ and is given by, $\langle \sigma v \rangle n_{dm}$. The factor $\langle \sigma v \rangle$, is the thermally averaged annihilation rate coefficient multiplied by the DM velocity. The result of the above multiplication by the DM number density has units of number of DM annihilation's divided by time.

Ref [13] also claims that if one considers the radial dependence of DM velocities, that a self-consistent way of producing the DM velocity dispersion is using the Jeans equation [18, 19]. Their theoretical model is then capable of producing a value for photon flux as measured at Earth

using:

$$\Phi = \int I(l,b)\mathrm{d}\Omega, \tag{2}$$

where I is a function representing the intensity distribution, containing an integral over the line of sight parameter, which depends on the Galactic longitude and latitude, b and l. Ref [20] then compared their theoretical model to intensity maps from INTEGRAL in the range of $|l| <60°$, $|b| <50°$. They also compared the expected flux to SPI for four different density profiles and varied the slope and fit parameters for each case. Constraints on the morphology for the decaying scenario imply that the halo must be very cuspy (meaning $\gamma >1.5$), which is not observed [13]. It was shown by [13] that a scalar LDM (light dark matter) particle could fit the SPI data for a constant (not velocity dependent) cross-section if $\gamma = 1.03 \pm 0.04$. Although these results show that an annihilating DM scenario could fit the SPI data, they are highly dependent on a very cuspy density profile. In fact, more resent work has gone underway to show that the light WIMP scenario is highly disfavoured for additional reasons. Ref [14] compared the necessary thermal DM cross-section for the light WIMP annihilating scenario, $\langle\sigma v\rangle \simeq 3\times10^{-26}$ cm^3 s^{-1}, to the available cosmological data and found that this candidate is no longer viable as a 511 keV line contributor.

Ref [15] explored the XDM model in some detail and found that a DM particle capable of an excited state, that is 1-2 MeV above the ground state, may be able to explain both the cuspy profile and the necessary e^+ production rate observed in the bulge. They also mention that the "bleeding off" of energy required to produce the signal from the reservoir of energy available, given the XDM scenario, is negligible, even when considering the age of the universe. This further substantiates the viability of the XDM scenario. Since the XDM scenario allows for a much larger range of WIMP masses, it is interesting to consider how the ratio of the splitting to the mass (δ/M_χ) changes the morphology of the signal. Using the latest (at the time) SPI data, Ref [15], constrained this ratio using the slope of SPI measurements. Whereas the work by Ref [13], fit parameters involving in the DM profile and the corss-section, the XDM model additionally allows for one to fit to SPI data by modifying the DM mass.

We outline here, Ref [15]'s methodology to show how one might construct a model of XDM. It is firstly necessary to define the form of the thermally averaged cross-section. The radially-dependent form is written in general as [15]:

$$\langle\sigma v\rangle(\vec{r}) = \int d^3v d^3v' f(\vec{v},\vec{r}) f(\vec{v'},\vec{r})\sigma(v_{rel})v_{rel}, \tag{3}$$

where $f(\vec{v},\vec{r})$ is the phase space velocity distribution, which is a function of particle velocity and position $\vec{v}$ and $\vec{r}$. $\sigma(v_{rel})$ is the velocity dependent inelastic scattering cross-section, and v_{rel} is the relative velocity between two interacting DM particles. $\sigma(v_{rel})v_{rel}$ may then be defined as $\sigma(v_{rel})v_{rel} = \sigma_c\sqrt{v_{rel}^2 - v_t^2}$, where $v_t \equiv \sqrt{4\delta/M_\chi}$ (derived in Section III) is the threshold velocity required to excite one or more of the DM particles to the excited state. Any velocity less than v_t and a production of $e^- e^+$ pairs is not

possible. σ_c represents the constant DM scattering cross-section which, in the relativistic limit, the velocity dependent cross-section approaches. Ref [15] uses a standard Maxwell-Boltzmann velocity distribution which is normalized so that $\int^{v_{esc}} d^3v f(v,r) = 1$. Finally, they follow the procedure in Ref [21], and using various kinematic arguments regarding rotation curves of the MW, construct a DM density profile and a function representing the escape velocity. Integration over the line of sight with a multiplication of the DM number density,

$$\int_0^\infty \langle\sigma v\rangle(r)n^2(r)dl, \tag{4}$$

allows for a direct comparison with SPI data, since Eq. 4 represents the number of pair creations per area per time [15]. The slope of the pair intensity, seen when compared to the SPI data, in the inner 10° of the galaxy, as a function of galactocentric angle, showed that masses between 400-600 GeV could serve to approximate the observed morphology. One of the attractive features to the XDM model is the radial cut-off imposed by integrating the velocity distribution above a certain threshold velocity. This radial cut-off is a necessary ingredient if a theory is to explain the observations by INTEGRAL.

The J-factor J(Ω) [22],

$$J \equiv \int d\Omega \int_{l.o.s.} \rho_\chi^2(x)dx \tag{5}$$

can be thought of as a representation of the morphology of astrophysical flux in a region with a DM density profile ρ_χ. In s-wave DM annihilation, we take the velocity dependent part of the thermally averaged annihilation rate coefficient to be spatially independent. In Eq. 3 this would send $\sigma(v_{rel})v_{rel} \to \sigma v_{rel}$, where σv_{rel} is a constant. In the case of s-wave DM annihilation, the morphology of the astrophysical flux is entirely encoded in the J-factor [19]. For cases in which the DM cross-section within the thermally averaged cross-section is velocity dependent, this is no longer the case and the morphology is ultimately effected along the Galactic radius. We mention the J-factor expression now, since as we will see shortly, calculations of the all-sky flux due to XDM [12], can be thought of as a simple extension of the J-factor.

A detailed study of XDM has additionally been carried out by Ref [12], and a more recent SPI data set ($\sim$8 years of data) used, to constrain both the thermally averaged rate coefficient, and DM mass range for s-wave annihilation. Their goal was to improve upon earlier papers by comparing directly to a more recent SPI data, with intent of better constraining the morphology of the DM distribution.

For completion, Ref [12] tested their analysis against both the decaying and (inelastic) scattering or XDM scenario, even though results of earlier papers had shown the decaying channel to be highly disfavoured. They tested the ability of two different DM halo profiles to provide a good parametrization of the DM halo. The Einasto profile:

$$\rho = \rho_s exp\left(-\left[\frac{2}{\alpha}\left(\frac{r}{r_s}\right)^\alpha - 1\right]\right), \tag{6}$$

and the generalized NFW profile:

$$\rho(r) = \rho_s \frac{2^{3-\gamma}}{(r/r_s)^\gamma (1 + r/r_s)^{3-\gamma}}. \tag{7}$$

The former has the benefit of not producing answers at infinity for very small values of r. The parameter r is the galactocentric radius/distance, defined in spherical polar coordinates as,

$$r = \sqrt{R_0^2 - 2xR_0\cos(\theta) + x^2}, \tag{8}$$

where x is the line of sight distance, R_0 is the sun's distance to the GC, and θ is the angle between R_0 and the line of sight. The parameters α, γ, and r_s in Eq.'s 7 & 6 are typically fit to N-body simulation results (Via Lactea II in the case of Ref [12]). The DM density normalization factor, however, can be determined using the local DM density $\rho_\odot$ at the sun's radial position $r_\odot$.

Ref [12] provides an expression for flux calculation in both the scattering and decaying scenario. For a DM particle with mass m_χ, the flux of 511 keV emission due to decay can be evaluated from:

$$d\Phi = 2(1 - 0.75 f_{Ps}) \frac{d\Omega}{4\pi} \int_{l.o.s.} \frac{\rho(\ell)}{m_\chi \tau} d\ell, \tag{9}$$

while for DM self-annihilation, the expression appears as:

$$d\phi = 2(1 - 0.75 f_p) \frac{d\Omega}{4\pi} \int_{l.o.s.} \frac{1}{2} \frac{\langle \sigma v \rangle \rho^2(\ell)}{m_\chi^2} d\ell. \tag{10}$$

Eq. 10 acts like an extension of the J-factor mentioned earlier but has the correct units for a flux calculation. It should now be clear that so long as $\langle \sigma v \rangle$ remains a constant, the morphology is fully encoded within the J-factor. In both cases, ℓ parametrizes the line of sight and $f_{Ps} = 0.967 \pm 0.022$ is the positronium fraction, which is determined through observations (see Section II A). In the expression for decay, τ denotes the lifetime of the DM particle χ. In the annihilation expression, $\langle \sigma v \rangle$ denotes the thermally averaged annihilation rate coefficient discussed earlier in this section.

The factor of 0.75 in each expression implies that we are only concerning photons resulting from p-Ps formation, since the p-Ps state will produce two photons at 511 keV. The factor of 2 takes care of the fact that we demand two photons to be produced. The $1/2$ inside of the integral in the scattering expression is a statistical counting factor, used to account for the number of unique scattering events possible. The total number of unique scatterings, for N DM particles is $N(N-1)/2$. The factor of $1/2$ ensures we don't over count. Therefore, each expression calculates the flux of emission at a frequency of exactly 511 keV. Any diffuse continuum emission, or o-Ps spectrum must be determined through a different means than Eq.'s 10 & 9.

Furthermore, both expressions are more accurate, the closer positrons annihilate to their source. As explained in Ref [12], and mentioned earlier in Section II B, the problem of positron transport in the MW is far from resolved. However, Ref [12] proceeds with the assumption of minimal positron propagation through the MW due to a lack of experimental or theoretical evidence forcing them to assume otherwise.

The last major piece used to construct the model used by Ref [12], is the addition contributions from other astrophysical sources in the disk. Ref [1] explains that the most likely candidate for the observed spectrum may in fact be a combination of the candidates mentioned in Section II B. For example, the combination of disk emission from radioactive elements and a DM source might be a possibility. Ref [12] used both an old disk (OD) and a young disk (YD) model [23] to model additional flux of 511 keV emission from radioactive decay of the unstable ^{26}Al and ^{44}Ti isotopes. The flux from either Eq. 10 or Eq. 9 would then add linearly with the flux from the either of the disk models.

Ref [12] proceeded to use a maximum log-likelihood ratio (MLR) test to fit the parameters in both the disk component and the DM component of their theoretical flux model, when comparing their model to the SPI data. They performed two tests. The first, fixing the fit parameters in the DM density profiles to the those suggested by Via Lactea II, and varying the normalization coefficients in the disk models and the DM flux expressions. The second, allowing the fit parameters in the density profiles to also vary. The respective fits, using the Via Lactea II parameters, can be seen in Fig. 4. Visually, it is clear that that Einasto plus disk combination (scattering DM scenario) was able to provide the closest result to the reconstructed SPI data. The MLR ratio was also found to be the greatest for this case. When varying the fit parameters in the Einasto density profile, they saw little change in the MLR, indicating that the Via Lactea II parameters likely provide a good representation of the DM halo if scattering DM is found to be an accurate scenario.

The best fit, thermally averaged cross-section for annihilation (taken to be a constant), was found by Ref [12] to be $\langle \sigma v \rangle = 5.1 \times 10^{-25} (m_\chi/\text{GeV})^2$ cm^{3}s^{-1}. From this estimate, one can calculate the range of $\langle \sigma v \rangle$ for a range of masses. Ref [12] explains that if the mass of a WIMP is in the range of 10-1000 GeV, the cross-section $\langle \sigma v \rangle$, would have a corresponding range of 10^{-23}-10^{-19} cm^{3}s^{-1}. For reference, this range is above the necessary cross-section of 3×10^{-26} cm^{3}s^{-1} required to achieve the observed relic density of DM, however as Ref [12] explains, the physical process here is not direct annihilation. It is scattering to an excited state and therefore allows for a larger cross-section since the de-excitation will result in a DM particle once again.

In this work, the thermal annihilation cross-section was taken to be independent of Galactic radius. The fact that the velocity dispersion may be peaked toward the bulge [12], may mean that the cross-section is largely effected for regions close to, or inside of the bulge. Including this radial dependence could result in a morphology and total flux, that is more peaked toward the bulge, similar to what was found by Ref [15], due to the radial cut-off imposed by the threshold velocity. In fact, in the remainder of this paper, we examine the case of adding a radial dependence to $\langle \sigma v \rangle$, with the goal of considering the change in morphology Ref [12] was not able to, with their model.
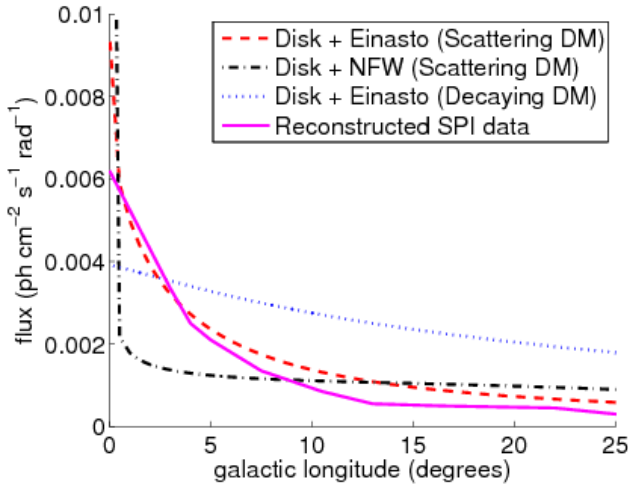
Figure 4. Theoretical photon flux as a function of galactic longitude for scattering and decaying DM models with different DM density profiles. "Disk" refers to disk components from radioactive isotopes. Overlaid is reconstructed SPI data for comparison. From [12].

III. THEORETICAL MODEL

In this section, we begin outlining our contributions to what has been done on the topic axis at the present time. Specifically, we develop in this section our theoretical model used to build upon the results from Ref [12]. In our present work, we incorporate a radial dependence in the thermal annihilation rate coefficient. We do this by invoking a threshold velocity limit which relative DM particles must achieve in order to reach the excited state. As we will see, this can be thought of as s-wave annihilation, but which is screened by the radial dependence of the DM velocity distribution. This sets an implicit velocity dependence on the DM cross-section, σv_{rel}, inside of $\langle \sigma v \rangle$. Therefore, we are assuming a model which proposes that DM may be capable of an excited state, for which the excitation and de-excitation, results in a $e^- e^+$ pair. This is the XDM model. We have outlined the reasons for which this model may be effective where other models have failed to account for the observed 511 keV emission spectra. We will present a working theory which helps constrain the DM cross-section and the DM mass with the use of the latest INTEGRAL/SPI data.

A. DM Distribution in the MW

We follow a similar procedure to Ref [12] by beginning with a NFW profile [16] to model the shape of the MW DM halo. This profile was given in Eq. 7 in Section II C. This is mostly out of simplicity and because earlier studies [12, 13, 22] have been able to achieve trustworthy results with a NFW parametrization. The fit parameters were chosen to agree with the initial analysis of [12]. These are the parameters corresponding to the Via Lactea II simulation and are $\gamma = 1.2$ for the slope parameter and $r_s = 26.2$ kpc. ρ_s is then calculated in our analysis using $\rho_\odot = 0.4$

GeV cm^{-3} at the suns position $r_\odot = 8.5$ kpc as outlined in Section II C.

Calculation of the escape velocity of DM particles is necessary to determine the upper limit of integration on the integral in $\langle \sigma v \rangle$ (see Eq. 20). Given the gravitational potential that a given DM particle will experience, the escape velocity is straight forward to calculate [19]. For a spherically symmetric distribution, the gravitational potential is easy to determine. The MW baryonic distribution is not spherically symmetric and therefore requires a more complicated distribution. For simplicity, we use a symmetrized version of both the disk and the bulge potentials representing the baryonic matter distribution. The gravitational potential then takes the form [19]:

$$\Phi_{bulge}(r) = -\frac{G_N M_b}{r + c_0}, \qquad (11)$$

when considering potential from baryonic matter in the bulge. Far from the center of the MW, we assume the potential from baryonic matter alone, takes the form of a spherical disk potential:

$$\Phi_{disk}(r) = -\frac{G_N M_d}{r} \left(1 - e^{-r/b_d}\right). \qquad (12)$$

In both Eq.'s 11 & 12, $G_N = 6.67 \times 10^{-8} \text{cm}^3\text{g}^{-1}\text{s}^{-2}$, is the universal gravitational constant. In the bulge potential, $M_b = 1.5 \times 10^{10} M_\odot$ is the bulge mass and $c_0 = 0.6$ kpc is the bulge scale radius, while in the disk potential, $M_d = 7 \times 10^{10} M_\odot$ is the disk mass and $b_d = 4$ kpc is the disk scale radius.

The DM halo has been shown to have a large amount of spherically symmetry. For a mass distribution described by a spherical density profile, the Poisson equation in Newtons theory of gravity,

$$\Delta^2 \phi(r) = 4\pi G \rho(r), \qquad (13)$$

can be used to determine the gravitational potential via [24]:

$$\phi(r) = -4\pi G_N \left(\frac{1}{r} \int_0^r \rho(r') r'^2 dr' + \int_r^\infty \rho(r') r' dr' \right). \qquad (14)$$

Another, perhaps more intuitive way of determining the gravitational potential is directly from the formula defining the gravitational potential from Newtons theory. We assume that the DM halo is spherically symmetric [13] and compute the DM gravitational potential via:

$$\Phi_{DM}(r) = \int_\infty^r \frac{G_N M_{enc}}{r'^2} dr', \qquad (15)$$

where M_{enc} represents the mass enclosed within a spherical shell of radius r. The integration to r from infinity takes care of the negative sign we expect to result in front ϕ_{DM}, since the potential is largest at infinity. The mass enclosed is calculated in the typical way, by integrating over the density profile to a radius r:

$$M_{enc} \equiv \int_0^r 4\pi r'^2 \rho_{NFW}(r') dr', \qquad (16)$$

where ρ_{NFW} represents the generalized NFW profile. It follows [19] that the escape velocity $v_{esc} = \sqrt{-2\Phi(r)}$ is determined with respect to the sum of the potentials, where $\Phi(r) \equiv \Phi_{bulge}(r) + \Phi_{disk}(r) + \Phi_{DM}(r)$.

We plot each of the potentials separately in Fig. 5 for radii in the range of $[10^6, 10^{24}]$cm. This range nicely shows the logarithmic dependence each of the potentials have on the radius. The disk potential is slightly more nuanced for radii $\lesssim 10^6$cm, though Φ_{DM} and Φ_{bulge} dominate for the inner radii so the behaviour of the disk potential is less important to consider there. The total escape velocity, along with the hypothetical escape velocity for each of the potentials is shown for radii in the range of $[10^{16}, 10^{25}]$cm in Fig. 6. This range provides a good representation of the escape velocity "fall-off" point. The escape velocity corresponding to Φ_{disk} is similarly nuanced for small value of r in this case as well, owing to the definition of v_{esc}.
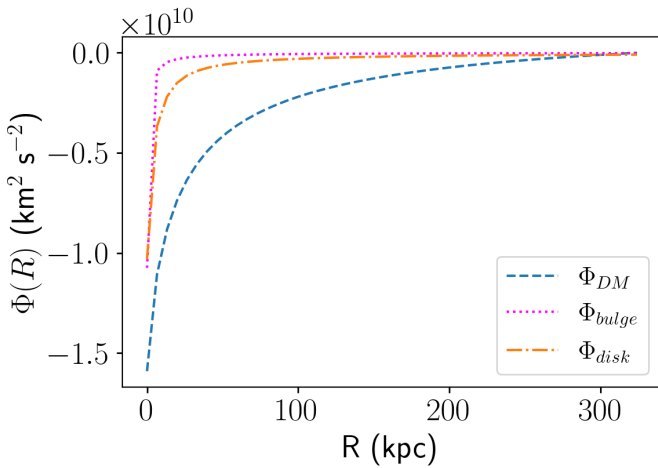

Figure 5. Potential functions describing the gravitational potential due to mass from DM, the Galactic bulge and the Galactic disk as a function of Galactic radius.
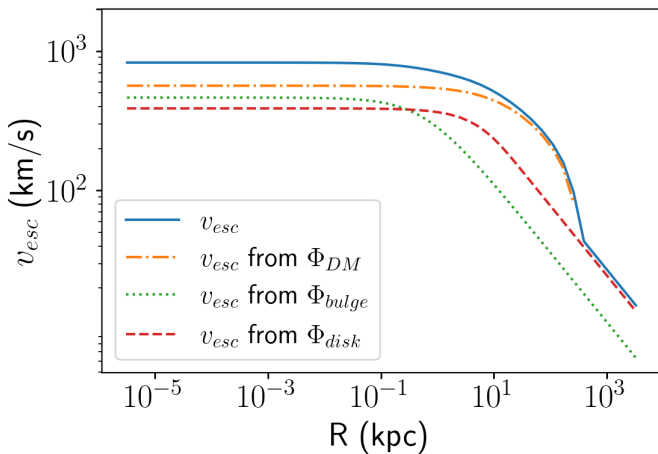

Figure 6. Escape velocities described by $v_{esc} = \sqrt{-2\Phi}$ for each of the potentials outlined in Fig. 5. v_{esc} from Φ_a, refers to the hypothetical escape velocity which is calculated using potential a alone, where $a \in [DM, bulge, disk]$.

B. Radially-dependent DM Cross-section

The thermally averaged annihilation cross-section in general, takes the form stated earlier (Eq. 3). In this section, we develop the form of the cross-section unique to our model, which incorporates a radial dependence that was overlooked by Ref [12]. Similar to what was done by Ref's [15, 25], we approximate the DM velocity distribution with an isotropic Maxwellwellian distribution for the sake of simplicity. This decision will help reflect the importance of the radial dependence of the dispersion velocities $\sigma_v(r)$ [25]. A Maxwellian approximation is a rough estimate, since halo velocities are likely not isotropic in reality, though we expect this approximation to be sufficient for our work here. In general, we define the single particle velocity distribution as:

$$f(\vec{v}, \vec{r}) = N\exp(-\vec{v}^2/2\sigma_v^2), \qquad (17)$$

which is normalized so that $\int^{v_{esc}} d^3v f(\vec{v}, \vec{r}) = 1$. σ_v is the three-dimensional velocity dispersion which describes the statistical difference in velocities about a mean velocity at a given radius r. If the distribution of velocities are taken to be isotropic, the dispersion relation $\sigma_v(r)$ can be determined by solving the Jeans equation [18, 25]:

$$\frac{\mathrm{d}(\nu\sigma_v^2)}{\mathrm{d}r} + \frac{2\beta}{r}\nu\sigma_v^2 + \nu\frac{\mathrm{d}\Phi}{\mathrm{d}r} = 0, \qquad (18)$$

where $\nu(r)$ is the local stellar density, and $\Phi(r)$ is the gravitational potential which depends on the density of the system [18]. In the case of the current analysis, $\Phi(r)$ would simply be the sum of the gravitational potential from the disk, bulge, and dark matter. Solving the Jeans equation, leads to the dispersion relation which we have plotted as a function of Galactic radius in Fig. 7. Evidently, particle velocities in our model have a higher dispersion for distances of ~ 1kpc.
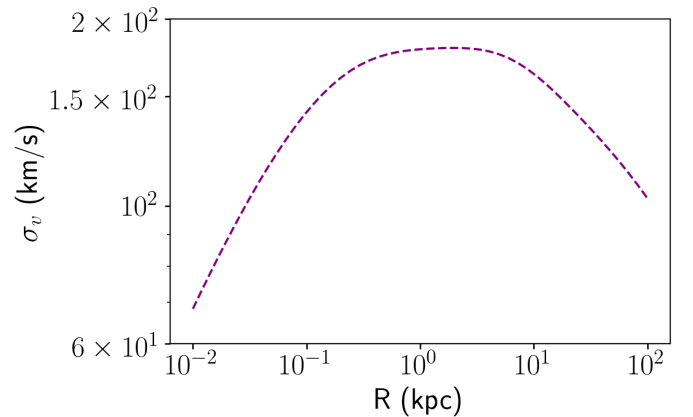

Figure 7. The 1D single particle velocity dispersion as a function of Galactic Radius. Values are found by solving for σ_r in the radial Jeans equation which is given in [18].

The velocity distribution defined in Eq. 17 corresponds to that of a single particle. We instead need a function which describes the velocity distribution of relative velocities ($\vec{v_{rel}} = |\vec{v} - \vec{v'}|$), since it is the relative velocities in a

center of mass frame which will ultimately decide whether a DM particle is excited to a higher energy state. We can convert Eq. 17 to an expression describing relative velocities by simply making the change of variables: $\sigma_v \to \sqrt{2}\sigma_v$. Note that we derive this in Section A. The relative velocity distribution thus takes the form:

$$f(\vec{v_{rel}}, \vec{r}) = N\exp(-\vec{v_{rel}}^2/4\sigma_v(r)^2), \qquad (19)$$

which, for reference, is plotted in Fig. 8.

At this point, we can use the generic form of the velocity-dependent annihilation rate coefficient to express the specific integral we need to evaluate. This becomes:

$$\langle\sigma v\rangle(r) = 4\pi N \int_{v_t}^{v_{esc}} v_{rel}^2\exp(-v_{rel}^2/4\sigma_v(r)^2)(\sigma v_{rel})\mathrm{d}v_{rel}. \qquad (20)$$

We have assumed an isotropic velocity distribution, so integration over θ and ϕ in spherical polar velocity space yields a factor of 4π, as seen in Eq. 20, and v_{rel} is no longer a vector containing three components. In general, although the annihilation cross-section term, $\sigma(v_{rel})v_{rel}$, is velocity dependent, we have chosen to re-write it as, (σv_{rel}). This is because we assume s-wave annihilation, and take this factor to be a constant free-parameter which will be fit to the SPI data.

The lower bound on the integral v_t represents the threshold velocity required for excitation above a given energy splitting. Formally, we assume there exists some threshold energy splitting, δE, between the ground and excited state of a DM particle. The collision must excite one or more of the particles undergoing the interaction. An excitation requires that the total kinetic energy in the center of mass frame be greater than the energy associated with the splitting. Assuming DM particles of equal masses, these arguments demand that,

$$\frac{1}{2}m_\chi\left(\frac{v_{rel}}{2}\right)^2 + \frac{1}{2}m_\chi\left(\frac{v_{rel}}{2}\right)^2 \geqslant \delta E \qquad (21)$$

$$m_\chi\frac{v_{rel}^2}{4} \geqslant \delta E \qquad (22)$$

$$v_{rel} \geqslant \sqrt{4\delta E/m_\chi}, \qquad (23)$$

where m_χ is the mass of a given DM particle. The radial dependence of $\langle\sigma v\rangle$ is now apparent in our model. By setting a lower bound on the integral, equal to the threshold velocity, we are screening the constant factor (σv_{rel}). One can think this case as a suppression of the constant, non-radially dependent cross-section, $\langle\sigma v\rangle$ used in Ref [12]'s model. The amount of suppression will then depend on the shape of the Maxwellian distribution and the threshold velocity. We expect this to result in a more cuspy morphology, since the radial cut-off will suppress flux in areas of lower average velocity, for a given distance from the Galactic center.

We now have all the tools we need to calculate the flux using Eq. 10. Setting (σv_{rel}) to a constant allows for the integral in Eq. 20 to be evaluated analytically and can be done using computer software. Maple produces the
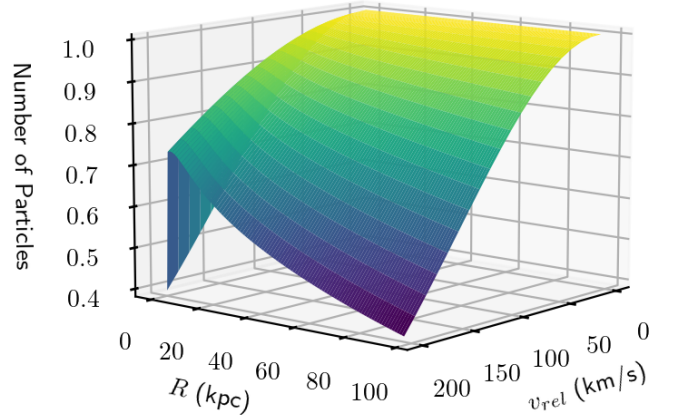

Figure 8. Normalized relative velocity distribution plotted for velocities in the range of 0-200 km/s and for a distance range of $\sim(10^{20}$ - $10^{23})$ cm.

following expression for the normalization coefficient:

$$N = \frac{1}{4\pi\left(-2v_{esc}\exp(\frac{-v_{esc}^2}{4\sigma^2})\sigma^2 + 2\sigma^3\sqrt{\pi}\mathrm{erf}(\frac{v_{esc}}{2\sigma})\right)}, \qquad (24)$$

where erf is a typical error function. The full analytical expression for $\langle\sigma v\rangle$ therefore appears as:

$$\langle\sigma v\rangle(r) = 4\pi N\left[2v_t\exp\left(-\frac{v_t^2}{4\sigma^2}\right)\sigma^2 - 2\sigma^3\sqrt{\pi}\mathrm{erf}\left(\frac{v_t}{2\sigma}\right)\right.$$
$$\left. - 2v_{esc}\exp\left(-\frac{v_{esc}^2}{4\sigma^2}\right)\sigma^2 + 2\sigma^3\sqrt{\pi}\mathrm{erf}\left(\frac{v_{esc}}{2\sigma}\right)\right], \qquad (25)$$

where N has been given in Eq. 24. The flux integral now appears with the slight radial-dependence modification to the annihilation rate coefficient,

$$d\phi = 2(1 - 0.75f_p)\frac{d\Omega}{4\pi}\int_{l.o.s.}\frac{1}{2}\frac{\langle\sigma v\rangle(r)\rho^2(\ell)}{m_\chi^2}d\ell, \qquad (26)$$

and is composed of analytical expressions, with the exception of the line of sight and solid angle integrals. The all-sky flux, for a given m_χ, is therefore straightforward to calculate given Eq. 26. One benefit of this model is that fluxes from multiple sources are expected to add linearly. For example, we could include at this point in our development, a model for contributions from radioactive isotopes in the disk, or even another source contribution. The total flux would simply be the sum of the flux from the contributions and the flux from DM.

Eq. 26 should be independent of the coordinate system used. Therefore, although a spherical coordinate system provides a tidy expression for the Galactocentric distance

(it helps that r is independent of the ϕ angle), conversion to Galactic coordinates b and ℓ is necessary for comparison with the SPI data in Ref [26]. Plotting the flux as a function of Galactic longitude, provides the most visual representation of the morphology of the signal. Fortunately, the Galactocentric distance r and the solid angle fully encode any information regarding a change of coordinates. In Galactic coordinates, we note that:

$$
\begin{aligned}
x &= dsin(b) \\
y &= dcos(b)sin(\ell) \\
z &= dcos(b)cos(\ell),
\end{aligned}
\tag{27}
$$

so that the Galactocentric distance can be written as:

$$
r = \sqrt{d^2 + R_0^2 - 2R_0 dcos(b)cos(\ell)},
\tag{28}
$$

where d is the line of sight distance (as measured from the earth) and R_0 is the suns distance to the Galactic center. The solid angle in Galactic coordinates is thus:

$$
d\Omega = cos(b)dbd\ell.
\tag{29}
$$

With the development outlined in this section, we are now ready to compute the total expected flux from a DM source and compare to data from INTEGRAL/SPI.

IV. RESULTS

Since our results are entirely based off of numerical analysis, we required some way of testing the trustworthiness of our model along the way. We therefore began by using our model to reproduce results from earlier papers (eg. Ref's [12, 22]). In the following section (Sec. IV B), we outline the results of our contributions to earlier models with the model developed in the last section.

A. Confirming Results of Numerical Analysis

We began by computing the J-factor in polar coordinates using the parameters outlined in [22], which include halo parameters from the best fit values of [27]. These are R_0 = 8.127 kpc, $\rho_\odot$ = 0.4 GeV cm^{-3}, γ = 1.2, and r_s = 20 kpc. The J-factor provides a framework for numerically calculating the larger flux integral (Eq. 26) and therefore provides a good starting point to verify that our numerical integration method is working. We used the Scipy integration package in Python to perform the numerical integration. Numerically integrating the all-sky J-factor in spherical polar coordinates produced a value of $\sim 2.308\times10^{23}$ GeV^{-2} cm^{-5} sr, which is in almost perfect agreement with the result quoted in [22] for s-wave annihilation.

Constructing the flux integral simply requires one to add the necessary pieces to the existing J-factor integral. The result of Eq. 26 will then have units of flux. We thus constructed the full integral representing the flux from a DM source. Our model allows for easy comparison to Ref [12]'s results, since setting the threshold velocity to 0 should recover the full value for the cross-section which is taken to

be constant. Ref [12] uses halo parameters corresponding to the Via Lactea II simulation. In correspondence with this, we set γ = 1.2 and r_s = 26 kpc. Ref [12] also set the Earth-sun distance, R_0 = 5.5 kpc. We additionally set $\langle\sigma v\rangle$ = 8.2 $\times$ 10^{-26} $(m_\chi/\text{GeV})^2$, in agreement with Ref [12]'s best fit while using the NFW profile only (no disk contribution). Our all-sky flux calculation returns a value of $\sim3.64\times10^{-4}$ photons cm^{-2} s^{-1}. This result unfortunately differs from the result, 6.72×10^{-4} photons cm^{-2} s^{-1}, found in [12] by roughly a factor of two, computed using the same flux expression and parameters.

Using a lower scale radius of r_s = 12 kpc, in accordance with Ref [12]'s best fit result when varying all parameters, we achieve a flux of $\sim6\times10^{-4}$ photons cm^{-2} s^{-1}, which is much closer to the all-sky flux in [12] for this scenario. We attribute this discrepancy to our data set involving the dispersion velocities at the present time. When integrating our flux expression, we seem to achieve the same answer when integrating the line of sight integral from $0 \to \infty$ and from $10^{19} \to \infty$ (in units of cm). Since our dispersion velocities are only in the range of $\sim (10^{20}\text{-}10^{23})$cm, we believe this could result in a lack of flux from sufficiently low values of dispersion velocities for correspondingly small radii. We return to this point in Sec. V

Nevertheless, we proceeded with this discrepancy in mind and tested the capability of our model to produce similar morphological results to those found by Ref [12]. We kept the energy splitting (and subsequently v_t) at 0 and compared our calculated flux per radian, as a function of Galactic longitude (see Fig. 4) to the reconstructed SPI data from [12]. The result of our model can be seen in Fig. 9. The dashed blue line, representing our theoretical flux from DM alone agrees well with the same line corresponding to a NFW profile in Fig. 4. The suppression of flux for $\ell \gtrsim 10°$ is likely caused by the lack of a disk contribution in our model.
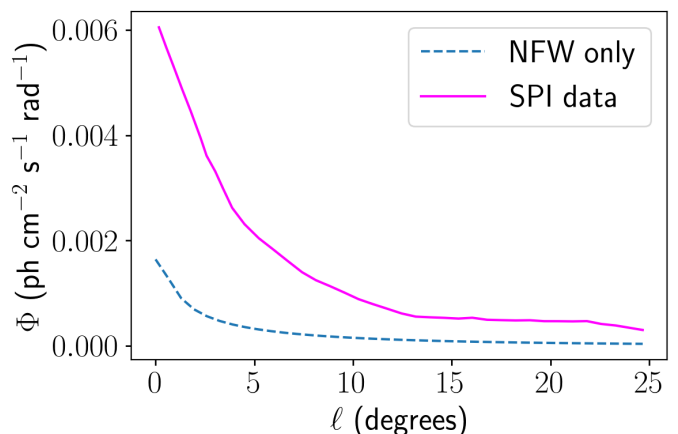

Figure 9. Dark matter profile as a function of Galactic longitude using our model with the threshold velocity set to 0. The SPI data is digitized from Ref [12]'s reconstructed SPI data. Galactic latitudes are in the range of [-15°, 15°] in our theoretical model to match what was done in [12].

B. Comparison with SPI Data

For a given set of halo parameters, our model allows for the varying of two main free parameters, the DM particle mass, m_χ, and the constant cross-section, (σv_{rel}), which appears inside of the integral in $\langle \sigma v \rangle(r)$. We set the energy splitting, δE, at 1.22 MeV, which is a reasonable choice since it corresponds to the rest mass of a $e^- e^+$ pair. It is worth noting that the energy splitting is also a parameter that can be varied, however $v_t = \sqrt{\delta E/m_\chi}$, so fixing the splitting and varying the mass or fixing the mass and varying the splitting have an analogous effect.

Using the halo parameters from the Via Lactea II simulation, we tested our numerical model against the results found by Ref [12] while allowing both (σv_{rel}) and m_χ to vary. We used two separate approaches to determine the best fit scenario. In the first approach, we used a manual least squares fit in one dimension to determine the most likely mass for a given constant cross-section. Our procedure involved manually adjusting the cross-section term and providing an array of masses to our function calculating the flux. We wrote a simple sub-routine which calculated the chi-squared statistic via:

$$\chi^2 = \sum_{bins} \frac{(T_i - E_i)^2}{E_i}, \qquad (30)$$

where T_i is the theoretical flux and E_i is the expected flux (SPI data) at the center of the ith bin. Our expected values consisted of the digitized data SPI data (reconstructed by Ref [12]), and our theoretical array was integrated over the corresponding values of ℓ (see caption of Fig. 9) with a length equal to the experimental array. We then simply found the corresponding m_χ for the minimum χ^2. This manual approach, although slower and far less accurate, has the added benefit of allowing us to plot the chi-squared statistic for a range of masses, providing a visual representation of the least squares fitting method. We repeated this procedure for the much more recent ($\sim$11 years of data collection) SPI data set used in [2, 26] and compared our results to the flux profile of a digitized longitudinal profile from [26].

Our procedure works by creating a two-dimensional grid with Galactic longitudes (ℓ) along the horizontal axis and Galactic latitudes (b) composing the vertical, where the integral along the line of sight has been computed inside each grid square. We then integrate using the trapezoidal technique along the b values to create a one-dimensional array that can be plotted as a function of the Galactic longitude, ℓ. Our digitized data from the $\sim$8 yr data set [12] has 39 points in the array, while our data from the $\sim$11 yr data set [26] contains 66 data points along ℓ. We are thus limited in the ℓ dimension by the number of grid points in each digitized array, but we can increase our resolution by increasing the size of our array corresponding to Galactic latitudes. For our analysis, we created an array of b values of length 20 for both data sets, meaning that our "resolution" for the grid when comparing to the $\sim$8 yr data was 39x20 = 780 grid points, while for the $\sim$11 yr data we had 66x20 = 1320 grid points.

For the comparison to the SPI data from [12], we found that an approximate best fit scenario worked if we set σv_{rel}

$= 1.0 \times 10^{-24}$ cm^3 s^{-1}. We then produced an array of 20 masses in the range of 13-18TeV, with $m_\chi \simeq 15894$ GeV providing the best fit with a chi-squared of roughly 0.0057. The best fit to the reconstructed SPI data and the corresponding chi-squared function can be seen in Fig.'s 10a & 10b. Performing the same analysis, but on the more recent data from [2], we found that for a DM constant cross-section of $\sigma v_{rel} = 9 \times 10^{-26}$ cm^3 s^{-1}, a mass of ~ 4263 GeV provided the best fit with a chi-squared of $\sim$0.067. This was found using an array of 20 masses in the range of 3-5 TeV. A plot of the fit to Ref [12]'s reconstructed SPI data and the corresponding chi-squared function are similarly shown in Fig's 10c & 10d.
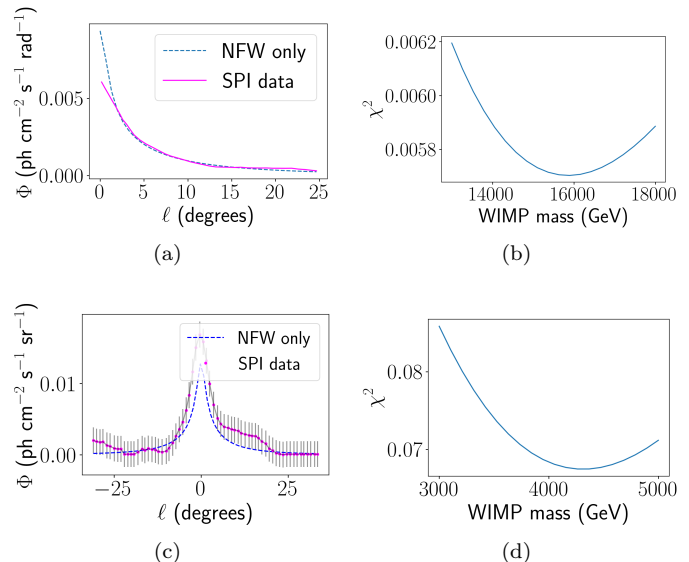

Figure 10. Longitudinal 511 keV line emission profiles for the best case scenario using our "manual" fit procedure and sub-routine. The chi-squared statistic function over a range of masses corresponding to each fit is plotted as well. (a) The best fit to a digitized data set from the reconstructed SPI data from [12]. (b) The corresponding chi-squared function for (a). (c) The best fit to the digitized (more recent) data set from [2] as plotted in [26]. The error bars have a height of 0.0018149 in units of the flux. (d) The corresponding chis-quared function for the fit in (c)

In our second analysis approach, we used Scipy's curve_fit package package and varied both the constant cross-section and DM mass simultaneously. This uses a least squares fit as well, so we are effectively preforming the same style of fitting procedure as in our manual estimate. We lose the ability to plot a representative chi-squared function but this approach is much quicker and far more accurate. By preforming a manual estimate first however, we gain the ability to make a more educated initial guess. We used the best fit results found for the fit in Fig. 10a as initial guesses for (σv_{rel}) and m_χ. Scipy's curve_fit's best fit scenario for the older data set [12] corresponded to $(\sigma v_{rel}) \simeq 4.30708 \times 10^{-24}$ cm^3 s^{-1} with a DM mass of $\sim$2861.12 GeV. The results of this fit can be seen in Fig. 11. Clearly the least fit regression technique from Scipy produces a visually good fit to the $\sim$8 year SPI data reconstructed by [12].

We finally constrained the DM mass and constant cross-

Data Set	Analysis Approach	DM Constant Cross-section (cm³s⁻¹)	m_χ (GeV)	Minimum χ^2
Digitized ~8 Yr Data	Manual Fit	1.0×10^{-24}	~ 15894	~ 0.0057
	Scipy	$\sim 4.3 \times 10^{-24}$	~ 2861	N/A
Digitized ~11 Yr Data	Manual Fit	9.0×10^{-26}	~ 4263	~ 0.067
	Scipy	$\sim 1.9 \times 10^{-25}$	~ 2861	N/A

Table I. Summary of best fit results using halo parameters consistent with the Via Lactea II simulation and Ref [12]'s analysis. These includes $\gamma = 1.2$ and $r_s = 26$ kpc. We show the results of both our manual fit estimates and the estimates mass and constant cross section (σv_{rel}) using Scipy's curve_fit procedure. The ~8 Yr data corresponds to the "reconstructed" SPI data from [12]. The ~11 Yr data corresponds to the data set used in [26] to produce the profile we fit to in Fig.'s 10c & 12.
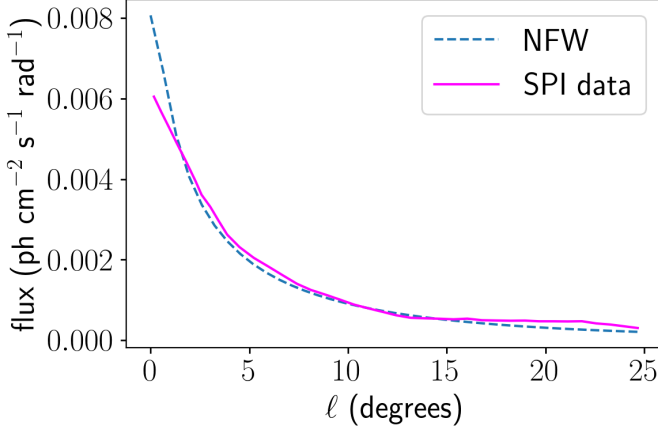

Figure 11. Theoretical longitudinal profile for the best fit scenario using Scipy's curve_fit package as the fitting method, fit to the reconstructed data from [12]. Galactic longitudes are in the range of $\pm 15°$
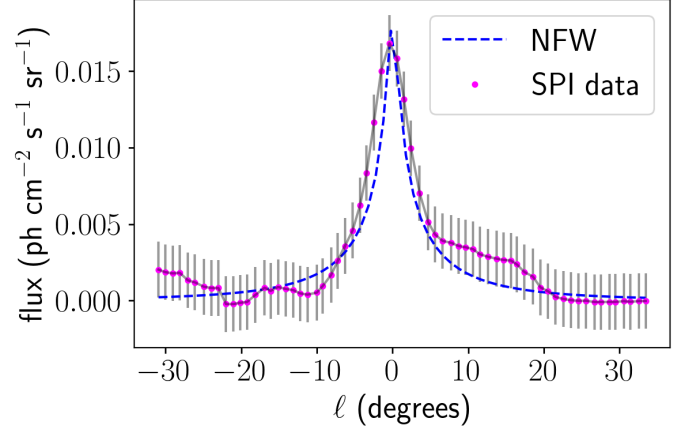
.

Figure 12. DM longitudinal 511 keV profile corresponding to our model's best fit to the 511 keV flux profile in [26], using Scipy's curve_fit procedure. Galactic latitudes are integrated over a range of $\pm 10.5°$. Error in the y-axis for the observed data is ± 0.00090745 in units of flux.

section by comparison with the latest data set from IN-TEGRAL/SPI which was used in [26] to produce a longitudinal profile for a wider range of ℓ. We performed this analysis above manually, however we also ran the Scipy curve_fit routine for the case of this much newer data set. In analogy with the older data set, we chose initial values for m_χ and (σv_{rel}) corresponding to those found with the manual fit procedure. These values can be found in Table I. Fitting our model data to the digitized data from the DM 511 keV profile found in [26], we found that a DM mass of $m_\chi \simeq 2861.14$ GeV with a constant cross-section of (σv_{rel}) $\simeq 1.91970 \times 10^{-25}$ cm³ s⁻¹. Our modelled longitudinal profile, constrained by the newer data set from [2], can be seen plotted against the 511 keV profile from [26] in Fig. 12. The least squares regression using Scipy clearly provides a better visual fit than our manual fit procedure when fit to the more recent data set. Our best fit parameters using the older [12] and newer data [26] show that the DM mass is the same to within 10 MeV, while the cross-sections differ by an order of magnitude. The summary of our fit results can be found in Table I. For completion, we plotted the all-sky intensity map (Fig. 13) using the parameters corresponding to the Scipy best fit procedure with the newer data set. The intensity map uses a "hammer" projection which preserves relative areas on the projected surface.

Using the best fit parameters for the DM mass and constant cross-section, we compared the total flux in the inner
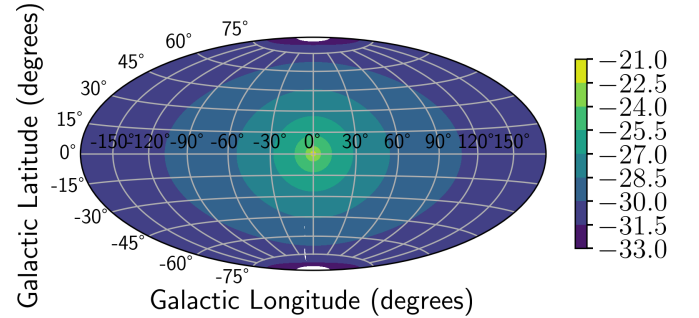

Figure 13. All-sky intensity map produced using the best fit parameters found with the Scipy fit to the data set from [2], used to construct the 511 keV profile in [26]. Uses a "hammer" (equal area) map projection. The natural log of the emission is shown to display more features of the intensity gradient. Therefore, the colorbar is in units of $ln(\Phi)$, where Φ is the flux from the 511 keV line.

$\sim 30°$ of the Galaxy to the same result found in [26]. We achieve a flux of $\sim 2.49 \times 10^{-3}$ ph cm⁻²s⁻¹ which disagrees, by roughly a factor of two, with Ref [26]'s total flux from the inner 30 degrees from both the small, $(1.2 \pm 0.055)10^{-3}$ ph cm⁻² s⁻¹, and the large, $(1.31 \pm 0.135)10^{-3}$ ph cm⁻² s⁻¹ regions of interest (ROI).

V. DISCUSSION

We provided a direct contribution to the model used in [12] by adding a radial dependence and an implicit velocity dependence to the thermally averaged cross-section of annihilation, $\langle \sigma v \rangle$. Without the inclusion of a disk model to simulate the contribution of radioactive injecta, our results refer specifically to the DM only contribution to the 511 keV line. Furthermore, our flux calculation provides the flux of line emission at exactly 511 keV and does not include any contribution to the o-Ps spectrum or the MeV continuum.

We found that using the halo parameters given in [22], we could re-derive the s-wave annihilation J-factor found in the same paper, but when we incorporated our radially dependent annihilation cross-section (Eq. 20), we could not achieve the same result as in [12] for the case of $\delta E = 0$. Using the same halo parameters as in [12], our calculated all-sky emission differed from the their result by a factor of ~ 2. Since we were using the same parameters, the case of zero energy splitting (this is the same as setting $v_t = 0$), and comparing to the "NFW only" case, our model should default to that of [12] in this limit. We estimate this to be the result of an incomplete set of dispersion velocities. In kpc, our dispersion velocities cover a range of 0.01-100. Our interpolation method for constructing the function $\sigma_v(r)$ therefore provides an approximate dispersion velocity for small values of r and may not accurately reflect the velocities in the bulge, where the emission flux is the largest. Moreover, our calculated all-sky flux is *less* than the quoted result by a factor of ~ 2. Since a lower than expected dispersion velocity at a given radius, would result in a lower velocity distribution at that same radius (see Eq. 19), we would expect a flux difference to be in the negative direction.

We found that our model flux, as a longitudinal profile did a reasonable job of approximating the 511 emission line when compared to both the set of older digitized SPI data from [12] and the more recent digitized data set from the profile in [26]. We neglected to include variations of our fits using different halo parameters, since using a similar model, this was not found to provide a largely better fit given the inelastic scattering scenario [12]. We also did not include measurements where we varied the energy splitting δE. Since it is the ratio of $\delta E/m_\chi$ which determines the threshold velocity, it should be clear that increasing the splitting, would result in a lower DM mass for the same v_t. We chose to use a reasonable choice of $\delta E = 1.22$ MeV, motivated by the rest mass energy of a $e^- e^+$ pair, however it could be that the splitting is larger or smaller in reality. This would be an interesting factor to explore more deeply in future work.

It is clear that our manual fit estimates are not worth much more than to provide a visual representation of the least squared regression method. Our masses found using this technique (~ 15 TeV for the ~ 8 yr data and ~ 4.2 TeV for the ~ 11 yr data) differ by a large margin, as do the constant cross-section terms. This discrepancy is likely due to the inability to sample a large enough data set manually, like is possible with a package like Scipy.

Our automated best fit procedure using Scipy's curve_fit

package, provided a DM mass that differed by only a factor of 10 MeV, when using each data set, implying that a DM particle would have a mass of ~ 2861 GeV if the XDM model and our work here is correct. This is still in the GeV-TeV that is compatible with the absence of a signal in direct detection experiments as explained in [1]. The fact that the cross-sections differ by an order of magnitude ($\sim 4.3 \times 10^{-24}$ cm^{3}s^{-1} for the older data and $\sim 1.9 \times 10^{-25}$ cm^{3}s^{-1} for the newer data), may be expected when we consider the shape of the data from each plot. The observed 511 keV line profile in Fig. 12 is more cuspy then the longitudinal profile in Fig. 11. The value of the constant cross-section term in the annihilation rate coefficient contributes to the cuspy-ness of our model profile. For example, the total flux becomes more sensitive to the radial cut-off imposed by the threshold velocity for a smaller (σv_{rel}), creating a more cuspy profile.

We found that the total flux in the inner 30° of the Galaxy, integrated over Galactic latitudes of height 21°, over approximated the flux by a factor of 2 in our model. In Fig. 12, many of the data points in the range of $|\ell| > 10°$ are very close to, or below zero. A negative flux is of course, not possible, however, the reconstructed data in [26] contains quite a bit of noise or random fluctuations in the signal for large Galactic longitudes. We believe that the inclusion of a disk model in our data could actually bring down the total flux in the inner 30 degrees since by bringing up the total emission in the disk, our modelled emission would become more cuspy, resulting in a smaller range of Galactic longitudes for which the emission is large. Integration over the inner 30 degrees could thus, result in less total emission.

Another factor which could have influence our model is our oversimplified form of $\langle \sigma v \rangle$. Although we incorporated the radial dependence into this parameter, we took the value (σv_{rel}) to be a constant parameter. A thorough approach is to fully incorporate the velocity dependence into the term we have taken to be constant and can be written as, $\sigma v_{rel} = \sqrt{v^2 - v_t^2}$ [15]. Clearly, in the relativistic limit, where v is large compared to v_t, this is not as important. Similarly, when v_t is 0 due to m_χ being large, or the energy splitting being 0 this is less important. However, if $v \sim v_t$, this term could have a large affect on the way $\langle \sigma v \rangle$ changes for different radii. We estimate that adding an explicit velocity dependence in the annihilation rate coefficient, could produce a more cuspy profile, and an overall suppression of emission as was found in [19]. This would be an interesting addition to our current model and is an area we would like to come back to.

VI. CONCLUSION

We have provided the motivation for the XDM model, which could serve to explain the excess 511 keV radiation in the Galactic center. Ever since the earliest observations of this emission line were able to produce enough data, the morphology and emission rate of the 511 keV line have provided a puzzling scenario for researchers. We can rule out radioactive injecta, small compact objects, and even the SMBH at the center of the Galaxy as possible individual

sources of this strange emission profile at the present time. It is possible however, that a combination of these sources, including a theory involving WIMPs, could be what is actually occurring.

Some of the earliest models involving DM as an origin to the 511 keV line, thought to include a decaying scenario, which has been since shown to be highly ruled out. We have provided an account of this here. Additionally, light WIMPs undergoing pure annihilation in flight are likely not the cause of the 511 emission line spectra. Instead, the assumption that DM is capable of an excited state, for which the excitation and de-excitation can result in a $e^- e^+$ pair, could serve as the best explanation. Not only does an XDM theory support the current WIMP mass range estimate, but it also supports the cuspy 511 keV longitudinal profile, which is observed.

Using a radially dependent annihilation rate coefficient, we have estimated the WIMP mass to be $\sim$2861 GeV, which does not entirely disagree with the expected WIMP mass range. Our results are highly dependent on positrons annihilating close to their source distribution, though this has been shown [1, 12] not to be a bad estimation. Our results, if anything show the capability of an XDM to fit both the morphology, and the expected emission rate of the observed 511 keV profile. With the modifications to our model, discussed in Sec. V, such as the addition of a disk model, we could have placed even tighter constraints on the expected WIMP mass if the XDM model is shown to be true. This is an exciting result and we hope to be able to make further refinements to our model, and perhaps be able to compare to a data set comprising an even longer range of data collection, in the future.

Appendix A: Relative Velocity Distribution Derivation

In this section, we derive the relation between the single particle velocity distribution and the corresponding relative velocity dispersion. The annihilation rate coefficient (Eq. 3) is proportional to the annihilation rate Γ, or:

$$\Gamma \propto \int f(\vec{v_1}) f(\vec{v_2}) d^3\vec{v_1} d^3\vec{v_2}. \tag{A1}$$

Our three dimensional single particle velocity profile is defined using a Maxwellian distribution as discussed in Sec. IV B. We define the quantity I as,

$$\begin{aligned} I &\equiv f(\vec{v_1}) f(\vec{v_2}) d^3\vec{v_1} d^3\vec{v_2} \\ &= \exp(-(\vec{v_1}^2 + \vec{v_2}^2)/2\sigma^2) d^3\vec{v_1} d^3\vec{v_2}. \end{aligned} \tag{A2}$$

We make a change of variables using the definition of v_{rel} and the center of mass velocity u. Therefore, we let,

$$\vec{v_{rel}} = \vec{v_1} - \vec{v_2} \quad \text{and} \quad \vec{u} = \vec{v_1} + \vec{v_2}. \tag{A3}$$

Writing $\vec{v_1}$ and $\vec{v_2}$ in terms of $\vec{v_{rel}}$ and $\vec{u}$, we have:

$$\vec{v_1} = (\vec{u} + \vec{v_{rel}})/2 \quad \text{and} \quad \vec{v_2} = (\vec{u} - \vec{v_{rel}})/2. \tag{A4}$$

Expanding the exponent, which we will define as E, in Eq. A2 by substituting the expressions in Eq. A4, we see that,

$$\begin{aligned} E &= -\frac{1}{2\sigma^2}\left(\frac{\vec{u}^2}{4} + \frac{\vec{v_{rel}}^2}{4} - 2\frac{\vec{u}\cdot\vec{v_{rel}}}{4} + \frac{\vec{u}^2}{4} \right. \\ &\quad \left. + \frac{\vec{v_{rel}}^2}{4} + 2\frac{\vec{u}\cdot\vec{v_{rel}}}{4} \right) \\ &= -\frac{1}{2\sigma^2}\left(\frac{\vec{u}^2}{2} + \frac{\vec{v_{rel}}^2}{2} \right). \end{aligned} \tag{A5}$$

Therefore,

$$I \propto \exp\left(-\left(\frac{\vec{u}^2}{2} + \frac{\vec{v_{rel}}^2}{2} \right)/2\sigma^2 z \right) d^3\vec{v_{rel}} d^3\vec{u}. \tag{A6}$$

We can further simplify Eq. A6 by realizing that an integration over $d^3\vec{u}$ would result in an extra constant in front and would not alter the functional dependence of the distribution on v_{rel} or σ. We are thus left with,

$$I \propto \exp(\vec{v_{rel}}/4\sigma^2) d^3\vec{v_{rel}}, \tag{A7}$$

implying that when we make the change from the single particle velocity dispersion to the relative velocity dispersion, we simply make the change of variables $\sigma \to \sqrt{2}\sigma$. Every other factor in the original velocity distribution remains unchanged. A graphical representation of the implication of this change of variables in shown in Fig. 14. From the definition of v_{rel}, we can see that on average, there should be a larger possible relative velocity. We therefore expect the relative distribution to be shifted slightly toward higher velocities, which is what is shown in Fig. 14. The increase in spread in the relative velocity distribution also makes sense, since there are more combinations of relative velocities given the velocities of two single particles alone.
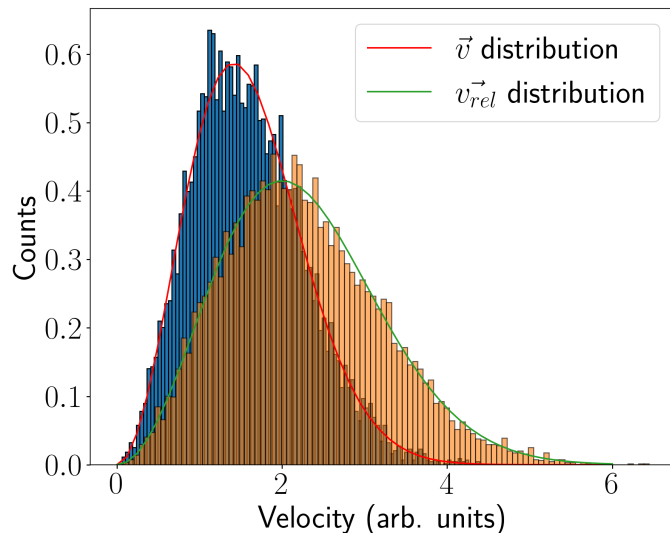
Figure 14. Check for comparison using a Monte Carlo simulation between the single particle velocity distribution and the relative velocity distribution. The normal velocity distribution is defined as a theoretical Maxwell Boltzmann speed distribution with $\mu = 0$ and $\sigma = 1$. The relative distribution uses the same parameters but with $\sigma \to \sqrt{2}\sigma$.

References

[1] N. Prantzos, C. Boehm, A. M. Bykov, R. Diehl, K. Ferrière, N. Guessoum, P. Jean, J. Knoedlseder, A. Marcowith, I. V. Moskalenko, and et al., "The 511 kev emission from positron annihilation in the galaxy," Reviews of Modern Physics **83**, 1001–1056 (2011).

[2] Thomas Siegert, Roland Diehl, Gerasim Khachatryan, Martin G. H. Krause, Fabrizia Guglielmetti, Jochen Greiner, Andrew W. Strong, and Xiaoling Zhang, "Gamma-ray spectroscopy of positron annihilation in the milky way," Astronomy &amp Astrophysics **586**, A84 (2016).

[3] J. Knödlseder, V. Lonjou, P. Jean, M. Allain, P. Mandrou, J.-P. Roques, G. K. Skinner, G. Vedrenne, P. von Ballmoos, G. Weidenspointner, P. Caraveo, B. Cordier, V. Schönfelder, and B. J. Teegarden, "Early SPI/INTEGRAL constraints on the morphology of the 511 keV line emission in the 4th galactic quadrant," Astronomy &amp Astrophysics **411**, L457–L460 (2003).

[4] J. Knödlseder, P. Jean, V. Lonjou, G. Weidenspointner, N. Guessoum, W. Gillard, G. Skinner, P. von Ballmoos, G. Vedrenne, J.-P. Roques, S. Schanne, B. Teegarden, V. Schönfelder, and C. Winkler, "The all-sky distribution of 511 keV electron-positron annihilation emission," Astronomy &amp Astrophysics **441**, 513–532 (2005).

[5] Marco Limongi and Alessandro Chieffi, "The nucleosynthesis ofsup26/supal andsup60/supfe in solar metallicity stars extending in mass from 11 to 120im/isub⊙/sub: The hydrostatic and explosive contributions," The Astrophysical Journal **647**, 483–500 (2006).

[6] M. Hashimoto, K. Nomoto, T. Tsujimoto, and F.-K. Thielemann, "Supernova nucleosynthesis in massive stars," International Astronomical Union Colloquium **145**, 157–164 (1996).

[7] K. Nomoto, N. Tominaga, M. Tanaka, K. Maeda, T. Suzuki, J. S. Deng, and P. A. Mazzali, "Diversity of the supernova-gamma-ray burst connection," Il Nuovo Cimento B **121**, 1207–1222 (2007).

[8] P. Martin, A. W. Strong, P. Jean, A. Alexis, and R. Diehl, "Galactic annihilation emission from nucleosynthesis positrons," Astronomy &amp Astrophysics **543**, A3 (2012).

[9] J. Daugherty and A. Harding, "Pair production in super-strong magnetic fields," ApJ **273** (1983), 10.1086/161411.

[10] S. Heinz and R. Sunyaev, "Cosmic rays from microquasars: A narrow component to the CR spectrum?" Astronomy &amp Astrophysics **390**, 751–766 (2002).

[11] H.-J. Grimm, M. Gilfanov, and R. Sunyaev, "The milky way in x-rays for an outside observer," Astronomy &amp Astrophysics **391**, 923–944 (2002).

[12] Aaron C Vincent, Pierrick Martin, and James M Cline, "Interacting dark matter contribution to the galactic 511 kev gamma ray emission: constraining the morphology with integral/spi observations," Journal of Cosmology and Astroparticle Physics **2012**, 022–022 (2012).

[13] Y. Ascasibar, P. Jean, C. B hm, and J. Knodlseder, "Constraints on dark matter and the shape of the milky way dark halo from the 511-kev line," Monthly Notices of the Royal Astronomical Society **368**, 1695–1705 (2006).

[14] Ryan J. Wilkinson, Aaron C. Vincent, Cé line Bœhm, and Christopher McCabe, "Ruling out the light weakly interacting massive particle explanation of the galactic 511 keV line," Physical Review D **94** (2016), 10.1103/physrevd.94.103525.

[15] Douglas P. Finkbeiner and Neal Weiner, "Exciting dark matter and the integral/spi 511 kev signal," Physical Review D **76** (2007), 10.1103/physrevd.76.083519.

[16] Julio F. Navarro, Carlos S. Frenk, and Simon D. M. White, "A universal density profile from hierarchical clustering," The Astrophysical Journal **490**, 493–508 (1997).

[17] A. Alexis, P. Jean, P. Martin, and K. Ferriè re, "Monte carlo modelling of the propagation and annihilation of nucleosynthesis positrons in the galaxy," Astronomy &amp Astrophysics **564**, A108 (2014).

[18] Thomas Richardson and Malcolm Fairbairn, "Analytical solutions to the mass-anisotropy degeneracy with higher order jeans analysis: a general method," Monthly Notices of the Royal Astronomical Society **432**, 3361–3380 (2013).

[19] Kimberly K. Boddy, Jason Kumar, and Louis E. Strigari, "Effective j -factor of the galactic center for velocity-dependent dark matter annihilation," Physical Review D **98** (2018), 10.1103/physrevd.98.063012.

[20] N. Guessoum, P. Jean, and N. Prantzos, "Microquasars as sources of positron annihilation radiation," Astronomy Astrophysics **457**, 753–762 (2006).

[21] David Merritt, Julio F. Navarro, Aaron Ludlow, and Adrian Jenkins, "A universal density profile for dark and luminous matter?" The Astrophysical Journal **624**, L85–L88 (2005).

[22] Carlos A. Argüelles, Alejandro Diaz, Ali Kheirandish, Andrés Olivares-Del-Campo, Ibrahim Safa, and Aaron C. Vincent, "Dark matter annihilation to neutrinos," Reviews of Modern Physics **93** (2021), 10.1103/revmodphys.93.035007.

[23] A. C. Robin, C. Reylé , S. Derrière, and S. Picaud, "A synthetic view on structure and evolution of the milky way," Astronomy &amp Astrophysics **416**, 157–157 (2004).

[24] Christopher J. Miller, Alejo Stark, Daniel Gifford, and Nicholas Kern, "Inferring gravitational potentials from mass densities in cluster-sized halos," The Astrophysical Journal **822**, 41 (2016).

[25] Brant E. Robertson and Andrew R. Zentner, "Dark matter annihilation rates with velocity-dependent anni-

hilation cross sections," Physical Review D **79** (2009), 10.1103/physrevd.79.083525.

[26] Thomas Siegert, Roland M Crocker, Roland Diehl, Martin G H Krause, Fiona H. Panther, Moritz M. M. Pleintinger, and Christoph Weinberger, "Constraints on positron annihilation kinematics in the inner galaxy," Astronomy & Astrophysics (2019).

[27] Maria Benito, Alessandro Cuoco, and Fabio Iocco, "Handling the uncertainties in the galactic dark matter distribution for particle dark matter searches," Journal of Cosmology and Astroparticle Physics **2019**, 033–033 (2019).